Mechanisms and Kinetics of Reduction of Solid NiO in CO/CO_2 and CO/Ar Gas Mixtures

JIANG CHEN and PETER C. HAYES

Experimental studies have been carried out on the reduction of dense nickel oxide in CO/CO_2 and CO/Ar gas mixtures at temperatures between 873 K and 1273 K (600 °C and 1000 °C). Examination of the nickel product microstructures of partially reduced samples has been undertaken using high-resolution scanning electron microscopy. It has been shown that the reduction can result in the formation of a dense nickel layer at the sample surface, continuous gas pore growth in the NiO, or the discontinuous growth of the porous nickel product. The product morphologies formed, and the microstructures of the gas/metal oxide/metal interfaces, are functions of reaction temperature and gas conditions. The microstructural and kinetic evidence indicates direct links between the reduction rates, nickel product growth mechanisms, and product microstructures.

https://doi.org/10.1007/s11663-019-01662-5

I. INTRODUCTION

THERE have been many studies examining the gaseous reduction of nickel oxide since the behavior of this system is of fundamental scientific interest as well of relevance to the industrial production of nickel metal. Most of the experimental studies of NiO reduction have been undertaken using hydrogen as the reductant; there have been relatively few studies of the reduction of solid NiO in CO/CO_2 gas mixtures and, as a result, the reaction mechanisms and kinetics of reduction in this system are poorly understood.

The formation and growth of Ni metal on the surface of dense NiO plates during reduction in flowing CO gas was observed directly using an optical microscope in conjunction with a hot stage apparatus.[1] The reduction was undertaken at temperatures from 873 K to 1273 K (600 °C to 1000 °C) in pure CO (1 atm.). At 973 K (700 °C) and below, following initial Ni nuclei formation and growth of a dense nickel metal layer on the NiO surface the rates of reduction were found to be drastically reduced. In contrast, in the same study, the complete reduction of NiO to Ni in H_2 was observed in the temperature range from 473 K to 1273 K (200 °C to 1000 °C). An experiment was undertaken at 673 K (400 °C) that involved switching the reactant gas from initially hydrogen to CO, then back to hydrogen. The sample was observed to reduce under the initial hydrogen H_2 atmosphere but no reduction was observed with CO; the reduction resumed when the H_2 was reintroduced into the system. The authors claimed that the reduction in CO was halted through the formation of Ni_3C, but this phase was not explicitly identified.

The reduction of pure NiO pellets, with open porosities ranging from approximately 3 to 37 vol pct, was carried out in CO/CO_2 gas mixtures at temperatures between 839 K and 1069 K (566 °C and 796 °C).[2] The temperatures and gas compositions were selected to ensure that no deposition of carbon or Ni_3C formation took place. This was confirmed by X-ray powder diffraction analysis of some of the pellets after reduction; these measurements verified the absence of carbon and of Ni_3C in the products. The rates and extents of reduction were measured by weight changes of the samples. The apparent reaction rates were estimated from the initial rates of reduction and were found to be first order with respect to CO partial pressure. The apparent activation energy between 839 K and 955 K (566 °C and 682 °C) was reported to be 196.5 kJ mol^{-1}; the reaction rate constants were found to be independent of temperature between approximately 953 K and 1069 K (680 °C and 796 °C).

The rates of reduction of NiO pellets in pure CO (1 atm.) were measured for temperatures ranging from 1120 K to 1272 K (847 °C to 1099 °C).[3] The porosity of the pellets was approximately 0.5. It was stated that after completion of the experiments, no evidence was found of C deposition. Although gas phase mass transfer to the particle surface was minimized by the use of high gas flow rates, it was not possible to

JIANG CHEN and PETER C. HAYES are with the PYROSEARCH, Pyrometallurgy Innovation Centre, School of Chemical Engineering, The University of Queensland, Brisbane, QLD 4072, Australia. Contact e-mail: p.hayes@uq.edu.au
Manuscript submitted February 16, 2019.
Article published online August 26, 2019.

eliminate the effects of pore diffusion within the sample itself; the grain model was used to interpret the experimental results obtained. The apparent activation energy for the rate constant for NiO reduction was reported as approximately 17 kJ mol^{-1} over the range of temperatures investigated.

Apart from the study by Reference 1, no detailed examination of the microstructural changes taking place during the reduction or the links to reaction kinetics in CO/CO_2 gas mixtures have been reported in the literature; this is the focus of the present study.

II. EXPERIMENTAL

The approach taken in the present study is designed to avoid any uncertainties associated with variable particle size, sample porosity and geometry, and potential variations in nucleation and reaction rate during reduction, by considering the reduction of dense NiO samples. The product microstructures are characterized by examining polished or fractured cross sections of the reaction product using optical and high-resolution scanning electron microscopy (SEM). The rates of reduction of the nickel oxide were determined by measuring the position of the reaction interface between nickel metal product and the original nickel oxide surface as a function of time.

The materials, methods of preparation of the NiO samples, and apparatus used for reduction have been described in detail in a previous publication.[4] In brief, high-purity nickel sheets (99.98 wt pct. Ni, Sigma-Aldrich, NSW, Australia) were oxidized at 1508 K (1435 °C) for 6 days in air. Each of the oxide sheets was mounted in epoxy resin and cut using a thin, diamond-bladed cut-off wheel, to obtain dense NiO samples with dimensions of approximately 2 × 2 × 1 mm. The individual samples were reduced in a specially designed apparatus, shown schematically in Figure 1.[4,5] An electric furnace was used to heat the reaction tube; the uniform hot zone was controlled within 2 K of the desired temperature. Before undertaking the experiments, the reaction tube was flushed with the reaction gas mixture to ensure the controlled reaction gas mixture was present throughout the experiment. A total gas flowrate of approximately 1 L min^{-1} was used in all experiments; this condition was based on the results of previous experimental studies using this apparatus using hydrogen gas as a reductant, which demonstrated that the reaction rates were not limited by gas phase mass transfer at these gas flow rates.

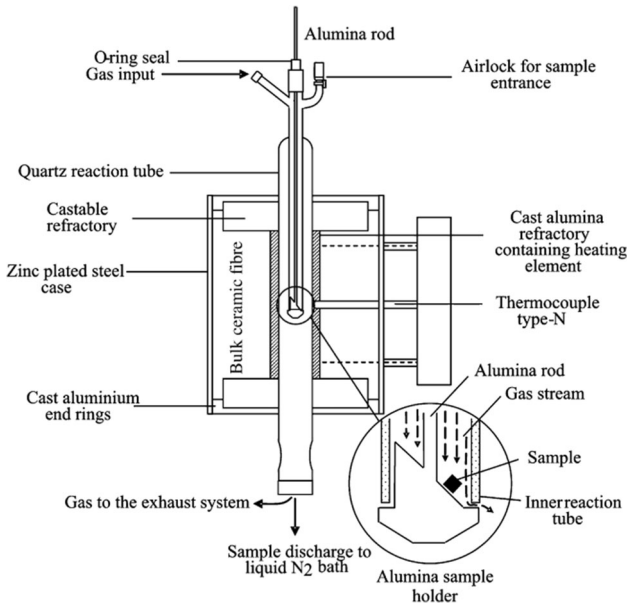

Fig. 1—Schematic representation of the reduction apparatus.[4,5]

The reduction experiments were undertaken in ($CO + CO_2$), ($CO + CO_2 + Ar$) and ($CO + Ar$) gas mixtures with a total pressure of 1 atm. High-purity (99.999 pct pure) gases were supplied as compressed gas by Coregas. The gas flows were accurately controlled using differential pressure gas flowmeters, and thoroughly mixed prior to introduction into the reaction tube by passing through a column filled with glass balls.[4]

Individual NiO samples were directly introduced into the hot zone of the quartz reduction tube through an airlock entrance at the top of the apparatus. The sample fell under gravity into the reaction tube into a fixed position in the uniform hot zone of the furnace onto a grooved alumina sample holder attached to an alumina rod. This sample position, and the narrow gap between the inner reaction tube and the sample holder, was designed to ensure maximum linear gas velocity over the sample surface during the reaction. After the required reduction period, the partially reacted sample was retrieved by lowering the alumina rod by several mm. The gap created between the sample holder and the inner reaction tube allowed the sample to fall under gravity to the liquid nitrogen quenching medium that was placed at the exit to the reaction tube. The use of liquid nitrogen provided both a thermal quench through cooling of the small sample and a chemical quench by creating a large volume of neutral nitrogen gas around the sample. In this way, the morphology of the sample formed at temperature was retained without change during the rapid cooling to room temperature.

Some samples were mounted in resin and cross sections were prepared for examination using optical microscopy using conventional metallographic techniques. Selected samples were sectioned by fracturing using a surgical scalpel and then examined using high-resolution Scanning Electron Microscope (SEM) JEOL JSM-7001F. In order to minimize the artifacts introduced during mechanical polishing, a focussed ion beam (FIB) FEI Scios DualBeam system—a combination of two systems: a Scanning Electron Microscope (SEM) and a Focused Ion Beam (FIB) system—was also used to prepare sections through the reaction product layer to reveal the interface between oxide and metal.

The experimental temperatures and gas compositions used in the present study are summarized in Table I. The Gibbs free energy or driving force for the reduction reaction was calculated in each case using the following relationship

Table I. Summary of Temperatures and ($CO + CO_2$) Gas Conditions Studied

Temp.	Reaction Conditions in ($CO + CO_2$) P_{tot} = 1atm. (Vol Pct CO)			K_{eq} ($NiO + CO$ = $Ni + CO_2$) Eq. [2]	K_{eq} ($2CO$ = $C + CO_2$ Eq. [3]	K_{eq} for $3NiO + 3CO$ = $Ni_3C + 2CO_2$ Eq. [4]	
600 °C	1.2	9.1	44.0	86.1	98.0	626	1.168 × 10	0.0065
700 °C	2.0	11.4	45.0	85.9	97.1	317.9	1.033	0.0015
800 °C	2.9	13.7	45.9	82.0	96.1	182.4	1.450×10^{-1}	0.0005
900 °C	3.9	15.9	46.8	80.4	95.0	114.8	2.874×10^{-2}	0.0002
1000 °C	5.0	18.0	47.5	78.9	93.9	77.6	7.408×10^{-2}	0.0000
ΔG (kJ mol^{-1} O_2)	− 30 (E)	− 60 (D)	− 90 (C)	− 120 (B)	− 150 (A)			

Equilibrium constants obtained from Ref. [6].

$$\Delta G = -2RT \ln\left[(pCO/pCO_2)_{gas}/(pCO/pCO_2)_{Ni/NiO}\right] \; J\ (mol\ O_2)^{-1} \quad [1]$$

where (pCO/pCO_2)gas is the CO to CO_2 ratio in the bulk gas and $(pCO/pCO_2)_{Ni/NiO}$ is the CO to CO_2 ratio at the Ni/NiO interface; the latter is equal to the equilibrium ratio.

The equilibrium constants for the reduction of NiO in CO/CO_2 are described by the following equation:

$$NiO(s) + CO(g) \rightarrow Ni(s) + CO_2(g) \quad [2]$$

The gas mixtures were selected so as to produce thermodynamic driving force for reduction of 30, 60, 90, 120, and 150 kJ mol^{-1} O_2 removed from the oxide (marked A–E in Table I) at the selected temperatures. The deposition of solid carbon is described by the reaction

$$2CO(g) \rightarrow C(s) + CO_2(g) \quad [3]$$

and the formation of nickel carbide, Ni_3C, through the reaction

$$3Ni\ (s) + 2CO\ (g) \rightarrow Ni_3C\ (s) + CO_2\ (g) \quad [4]$$

The equilibrium constants were obtained from Reference 6 all assuming 1 atmosphere pressure and pure solid compounds as standard states.

III. RESULTS

A. *Microstructural Changes*

Preliminary experiments undertaken as part of this study indicated that the rates of reaction of the gas with the NiO surfaces were extremely rapid; substantial changes in structure occurring within a matter of seconds. Since the focus of the present study is to determine the key reaction mechanisms taking place, the samples were selected for examination using scanning electron microscopy following relatively short reaction times, enabling nucleation, and growth of the nickel metal product phase to be followed.

1. *CO/CO_2 gas mixtures*

a. 873 K (600 °C) Examples of the surfaces of the NiO sample following reduction in CO/CO_2 gas mixture at 873 K (600 °C) (reduction potential B, ΔG − 120 kJ mol^{-1} O_2) after 30 seconds reaction are shown in Figures 2(a) through (d). Figure 2(a) shows that the smooth polished original surface has become facetted because of the reaction with the gas phase and the resulting selective removal of oxygen. Isolated pits are also formed, potentially the result of selective removal oxygen at emergent screw dislocations. It can be observed (Figure 2(b)) that the surface has decomposed locally into a network of instabilities; these instabilities spread across the oxide surface (Figures 2(c) and (d)) and appear to be associated with growth of porous nickel metal product.

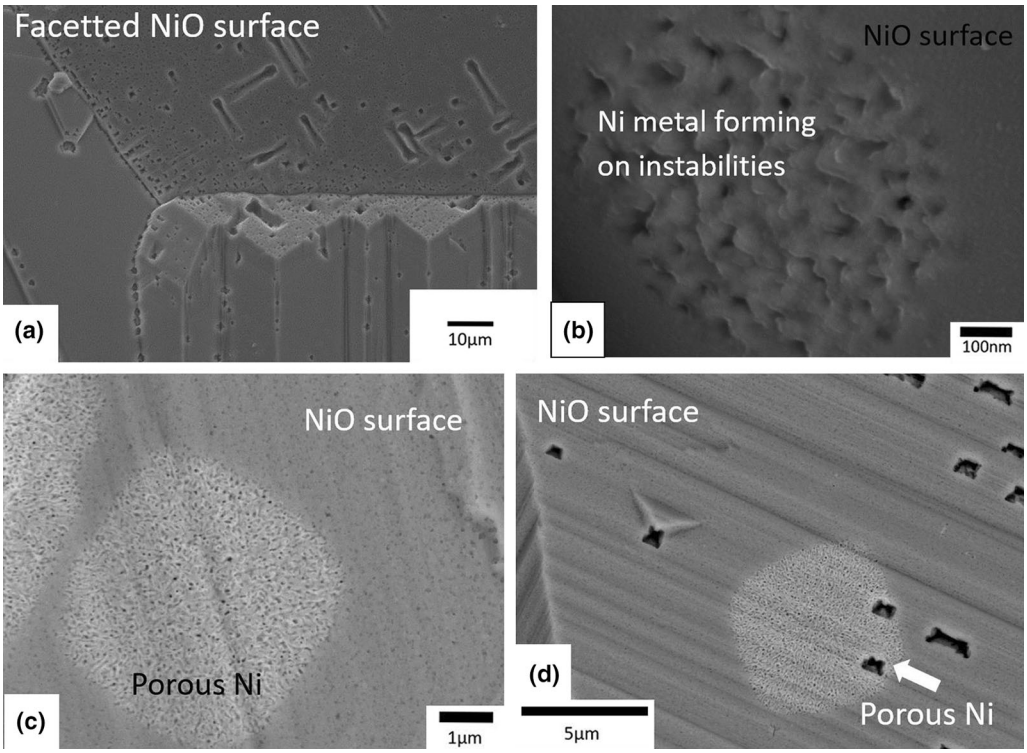

Fig. 2—SEM electron micrographs of the NiO surface during reduction in a CO/CO_2 gas mixture at 873 K (600 °C) reduction potential B, 30 s showing (*a*) facetting of the surface, (*b*) the formation of instabilities, and (*c*, *d*) porous nickel metal nuclei.

The growth of gas pores and the penetration of the reaction front into the NiO sample are illustrated clearly in cross sections of the samples given in Figures 3(a) through (c) for CO/CO_2 gas mixture at 873 K (600 °C) (ΔG − 150 kJ mol^{-1} O_2). In Figure 3(a), the interface at this high reduction potential looks macroscopically smooth. Figures 3(b and (c) show the formation of instabilities at the NiO surface and the development of isolated gas pores growing into the NiO.

Examination of the section prepared using the FIB (Figures 4(a) and (b)) in conjunction with backscattered scanning electron microscopy shows from the image contrast that there are regions of NiO behind the reaction interface that remain unreduced until some time after the main interface has passed. The image contrast also provides strong direct evidence that the surfaces of the gas pores are covered with a nickel metal layer.

b. 973 K (700 °C) The microstructures observed in samples reduced at 973 K (700 °C) ΔG − 120 kJ mol^{-1} O_2 (B) for 30 seconds exposure shown in Figure 5 are very similar to those shown in Figure 4. From the examples of the reaction interface as revealed by the backscattered FIB sections, it is clear that the interface is diffuse and that it consists of gas pores that penetrate from the samples surface into the original dense oxide; the pore tips range from 20 to 50 nm diameter; the distances between the pores are variable between 50 and 250 nm. Again, it appears that the surfaces of the pores are covered with a nickel metal layer. The backscattered electron images clearly show regions of unreduced NiO between the pores both at the growth interface and adjacent to the sample surface.

c. 1073 K (800 °C) Examples of the microstructure formed at 1073 K (800 °C) ΔG − 30 kJ mol^{-1} O_2, reduction potential E are shown in (Figures 6(a) and (b)). After a short reaction time, individual Ni metal nuclei are seen to form on the surface of the NiO; under these conditions after a reaction time of 30 seconds, the nuclei have grown to approximately 100 nm diameter and spacing 100 nm. After 5 minutes, the surface of the NiO is seen to be covered by a layer of dense nickel metal of approximately 10 nm thickness. Although the metal grains are of approximately 200 nm diameter, these appear to be covered by circular caps ranging from 20 to 50 nm in diameter.

An example of fractured sections taken from sample reduced at (Figure 7) ΔG − 90 kJ mol^{-1} O_2, reduction potential C shows that, under these conditions, the nickel product layer is porous and the reaction interface irregular in shape. The pores are equiaxed in shape, approximately 100 to 500 nm in diameter. In contrast to the structures at 1073 K (700 °C) shown in Figure 5, there is no evidence of residual NiO behind the reaction front.

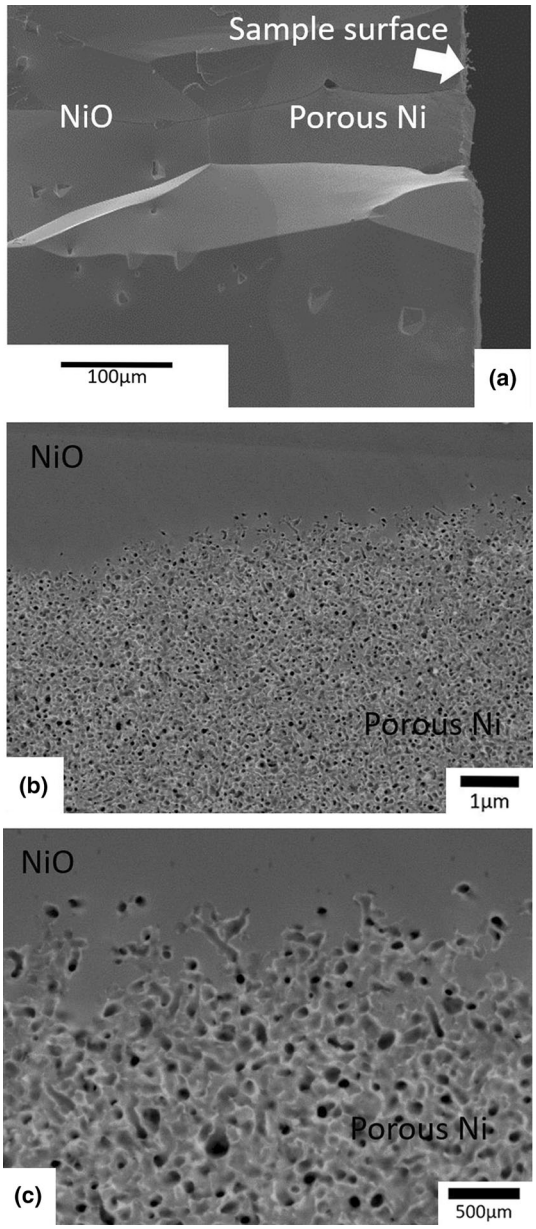

Fig. 3—(*a*) through (*c*) SEM electron micrographs of a polished cross section of partially reduced NiO during reduction in a CO/CO_2 gas mixture at 873 K (600 °C) reduction potential A, 5 min showing the formation of porous nickel metal.

d. 1000 °C The product structures formed at reduction potentials A–D at 1273 K (1000 °C) closely resemble those shown in Figure 7; at reduction potential E dense nickel metal layer was formed.

To clarify the differences between the dense and porous microstructures and their mechanisms of formation at this temperature, an experiment involving a two-stage reduction was undertaken at 1273 K (1000 °C). This procedure involved first reduction at ΔG − 30 kJ mol^{-1} O_2, reduction potential E for 60 seconds; the gas mixture was then changed to create ΔG − 150 kJ mol^{-1} O_2 reduction potential A. A micrograph of the sample surface having undergone this treatment are shown in Figure 8. It can be seen that the

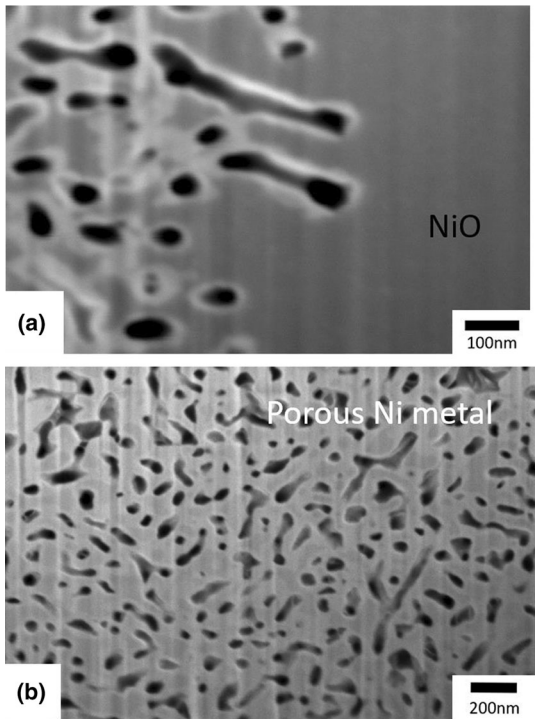

Fig. 4—SEM backscattered electron micrographs of a FIB-milled cross section of partially reduced NiO during reduction in CO/CO_2 gas mixture at 873 K (600 °C) reduction potential A, 5 min showing residual oxide (gray) present between nickel metal (white) covered gas pores, (*a*) gas reaction interface, and (*b*) in the partially reduced product layer.

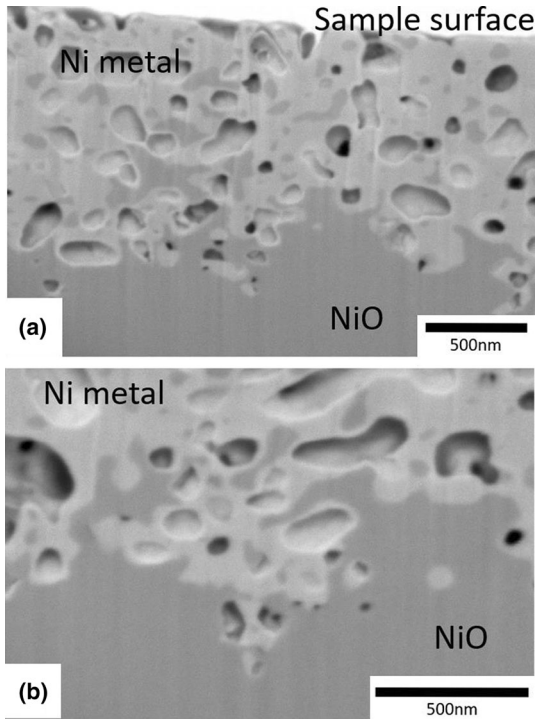

Fig. 5—(*a*, *b*) SEM backscattered electron micrographs of a FIB-milled cross section of partially reduced NiO during reduction in CO/CO_2 gas mixture at 973 K (700 °C) reduction potential B, 30 s, showing residual oxide (gray) present between the nickel metal (white)-covered gas pores.

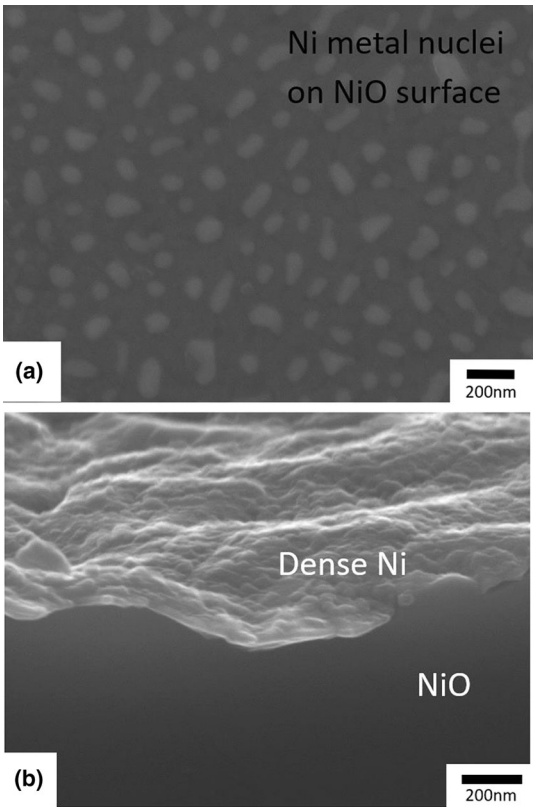

Fig. 6—SEM micrographs of partially reduced NiO during reduction in a CO/CO_2 gas mixture at 1073 K (800 °C) reduction potential E, 5 min showing (*a*) the formation of a dense nickel metal layer of the oxide surface and (*b*) fractured cross section of the sample.

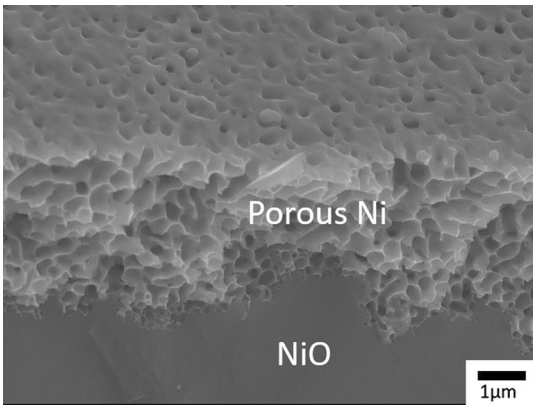

Fig. 7—SEM micrograph of partially reduced NiO during reduction in a CO/CO_2 gas mixture at 1073 K (800 °C) reduction potential C, 5 min showing the formation of porous nickel.

surface consists of a dense polycrystalline layer of nickel metal; grain size 1 to 3 μm diameter. Within this nickel layer are 1 to 5 μm diameter Ni circular caps, with some

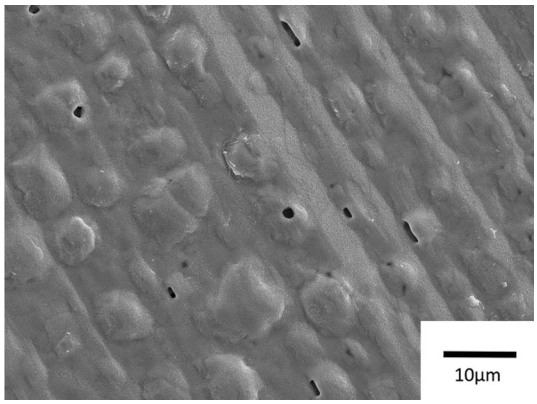

Fig. 8—SEM micrograph showing the surface of partially reduced NiO during reduction in CO/CO_2 gas mixtures at 1273 K (1000 °C), reduction potential E 60 s then reduction potential A 60 s, showing the formation of a dense nickel metal product layer followed by blistering and rupture of the layer.

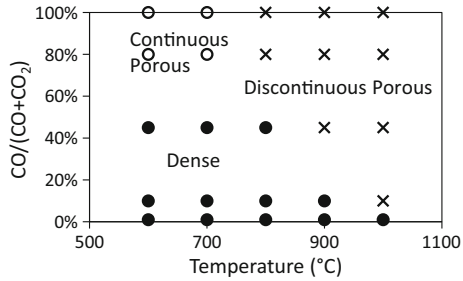

Fig. 9—Morphology map indicating the mechanisms of growth of nickel metal on reduction of NiO in CO/CO_2 gas mixtures as a function of CO partial pressure ($PCO + PCO_2 = 1$ atm.).

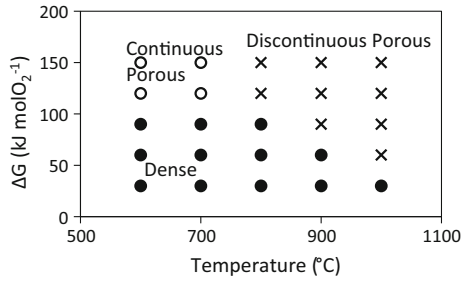

Fig. 10—Morphology map indicating the mechanisms of growth of nickel metal on reduction of NiO in CO/CO_2 gas mixtures as a function of thermodynamic driving force ($PCO + PCO_2 = 1$ atm.).

of these caps having holes in them, which allow the gas to access to the underlying porous product and NiO. This observation provides support for the view that growth of the porous nickel product layer takes place through a discontinuous growth mechanism in which successive bursting of metal layers takes place.

2. *Morphology maps*

Summaries of the microstructural types observed in the study are given in Figure 9, as a function of CO concentration and temperature, and Figure 10, as a function of thermodynamic driving force and temperature. The optical and electron micrographs show that a dense nickel metal product layer is observed between 873 K and 1273 K (600 °C and 1000 °C) at low CO concentrations and at relatively low thermodynamic driving forces for reduction. For example, below 1 pct CO in the gas phase, only dense nickel is formed; this is equivalent to reduction potential E.

Between 873 K and 1273 K (600 °C and 1000 °C) porous nickel product can be formed; however, the conditions under which porous product is obtained vary with temperature, and importantly different growth mechanisms appear to be active at the reaction interface under these different conditions. At 873 K and 973 K (600 °C and 700 °C) at reduction potentials A and B, gas pores are spontaneously created in the oxide through instability formation in the NiO. These pores form continuous pathways from the sample surface to the reaction interface, enabling the gas phase mass transfer of reactant gas through the product layer to the pore tip at the reaction interface. The sidewalls of the pores, those surfaces that are not located at the growing tip, are covered with layers of dense nickel metal.

Between 973 K and 1273 K (700 °C and 1000 °C) the experimental evidence indicates that porous nickel product can be formed through a discontinuous growth mechanism involving the successive formation and bursting of nickel metal layers; the gas conditions and reduction potentials at which this mechanism is active range between approximately A–D at 1273 K (1000 °C) and from A–B at 1073 K (800 °C).

In separate experiments involving $CO/CO_2/Ar$ with $(CO+CO_2)/Ar$ in the ratio of 1 to 4 and 1 atm. total pressure, dense nickel product layers were formed under all conditions, of reduction potentials A–E 873 K to 1273 K (600 °C to 1000 °C).

In experiments involving the use of CO/Ar gas mixtures between CO/(CO + Ar) 0.2 to 1.0 and 1 atm. total pressure, all resulted in porous nickel product except experiments at 973 K (700 °C) in which dense nickel layers were formed.

B. *Kinetics of Reduction*

In the present study, the rates of reduction of the nickel oxide were determined by measuring the position of the reaction interface between nickel metal product and the original nickel oxide surface as a function of time. These measurements were obtained from polished or fractured cross sections of the plate-like samples. This approach has some advantages and some limitations. Direct observation of the position of the interface means that the potential influence of cracks, grain boundaries and the corners of the plate-like samples can be avoided by taking measurements at distances away from these features. The samples were mounted at right angles to the polished sections to ensure that accurate measurement of the product thickness was obtained. Every effort was made in the experimental design to ensure the maximum rate of gas phase mass transfer to and from the sample surface. Any resistance to the transfer of reactant gas to the reaction interface will reduce the effective CO partial pressure and reduction potential. Any differences in gas phase transfer rates at different positions were detected by comparing the thicknesses of the product layer formed on all sides of the plate samples, which should be the same if gas phase mass transfer is not rate limiting. Uncertainties in the product layer thickness can arise from factors that are characteristic of the grain size and orientations, which cannot be readily controlled through experimental design. A typical example of the variation in Ni metal product thickness in the partially reduced samples is shown in Figure 3. Taking into account these sources of uncertainty, the maximum thickness of the product layer at positions away from cracks and from parallel interfaces was taken to be the more accurate reflection of the extent of reaction; the uncertainties of the thickness measurements were estimated to be ± 5 pct.

1. *CO/CO_2*

It has been shown in Figures 2 through 8 that the nucleation of nickel metal and coverage of the surface by nickel product takes place in a matter of seconds. The maximum rates of reduction of the dense NiO are therefore estimated from the apparent initial rate, the tangent of the thickness *vs* time curve at time, $t = 0$. The initial rates of reduction as a function of temperature in the range 873 K to 1273 K (600 °C to 1000 °C) for 100 pct CO, and given reduction potentials, ΔG − 150 (A), − 120(B), − 90 (C), − 60 (D) kJ mol^{-1} O_2, are given in Figure 11. It can be seen that the rates do not increase monotonically with increase in temperature. In fact, there is a decrease in rates for potentials in A and B between 873 K and 973 K (600 °C and 700 °C). Between 1073 K and 1273 K (800 °C and 1000 °C), the rates again increase with the increasing temperature. The rates at low reduction potentials are all slow in comparison; effectively, no reduction takes place at all

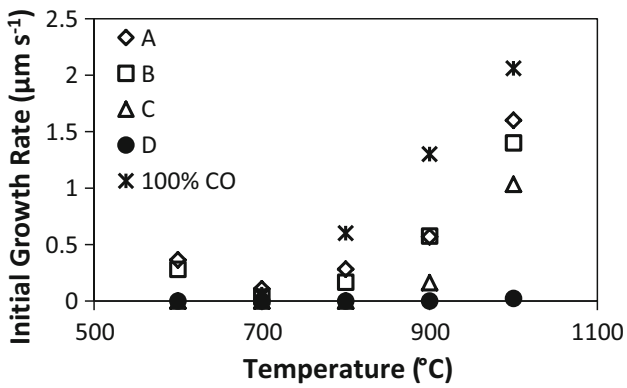

Fig. 11—Initial growth rates of nickel metal as a function of temperature on reduction of NiO in CO/CO_2 gas mixtures ($PCO + PCO_2 = 1$ atm.).

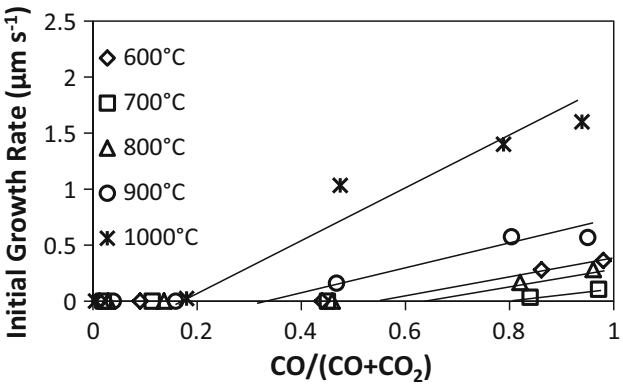

Fig. 12—Initial growth rates of nickel metal as a function of CO partial pressure on reduction of NiO in CO/CO_2 gas mixtures ($PCO + PCO_2 = 1$ atm.).

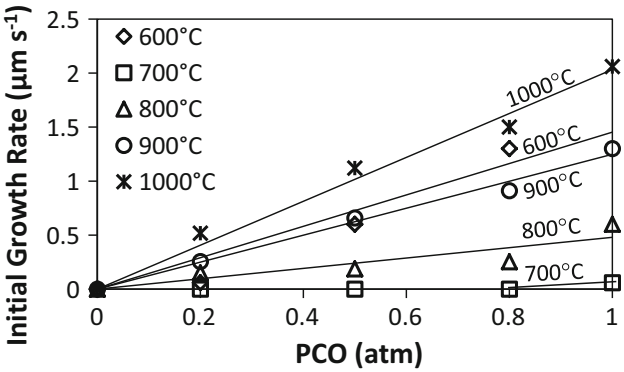

Fig. 13—Initial growth rates of nickel metal as a function of CO partial pressure on reduction of NiO in CO/Ar gas mixtures (PCO + PAr = 1 atm.).

temperatures under reduction potential E and all other conditions where a dense nickel product layer is observed.

The initial growth rates as a function of the CO partial pressure for ($CO + CO_2$) gas mixtures are given in Figure 12. It can be seen that the initial growth rates tends to zero as the transition from dense to porous nickel is approached at each temperature; these initial rates of product layer growth increase linearly with increasing CO partial pressure above these limiting values.

2. *CO/Ar*

Figure 13 shows the initial growth rates of the nickel product layer at 1073 K, 1173 K, 1273 K (800 °C, 900 °C, 1000 °C) for CO partial pressures of 0.2, 0.5, 0.8, 1.0 atm. for reduction in CO/Ar gas mixtures. It can be seen that the initial growth rates increase linearly with increasing CO partial pressure. A local minimum in reduction rate is observed between 873 K and 1073 K (600 °C and 800 °C). Initial growth rates of nickel metal product as a function of temperature for selected CO partial pressures on reduction of NiO in CO/Ar gas mixtures are given in Figure 14; the reduction rate

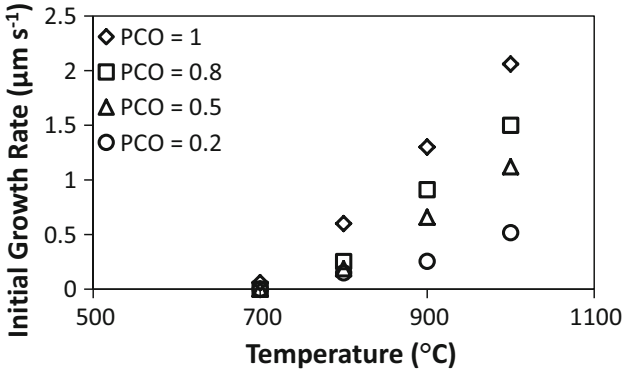

Fig. 14—Initial growth rates of nickel metal as a function of temperature on reduction of NiO in CO/Ar gas mixtures (PCO + PAr = 1 atm.).

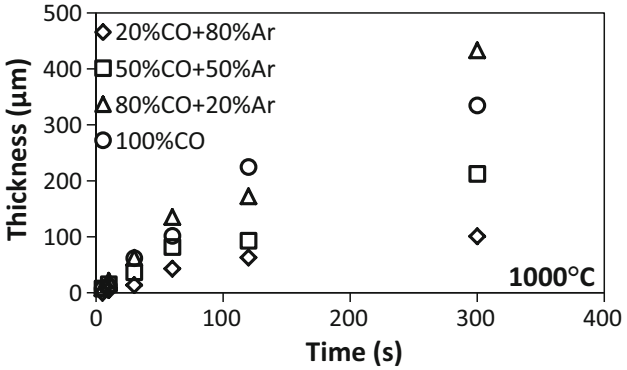

Fig. 15—Nickel metal product thickness as a function of time on reduction of NiO in CO/Ar gas mixtures at 1273 K (1000 °C) (PCO + PAr = 1 atm.).

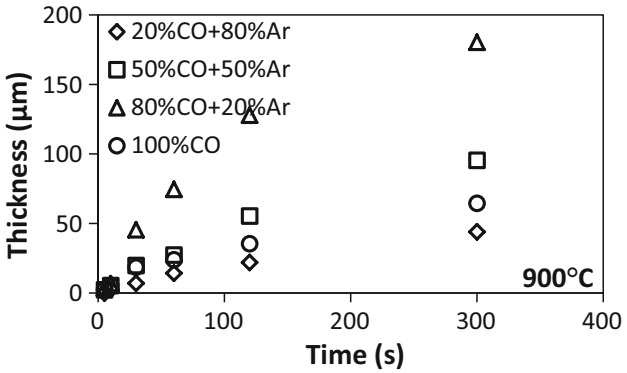

Fig. 16—Nickel metal product thickness as a function of time on reduction of NiO in CO/Ar gas mixtures at 1173 K (900 °C) (PCO + PAr = 1 atm.).

increasing with increasing temperature above approximately 973 K (700 °C). The results provided in Figures 12 (CO/CO_2) and 13 (CO/Ar) show that there are differences in the rates of reduction in CO/CO_2 and CO/Ar gas mixtures for the same CO partial pressure. Note the high thermodynamic driving for reduction is retained using CO/Ar as the CO partial pressure is

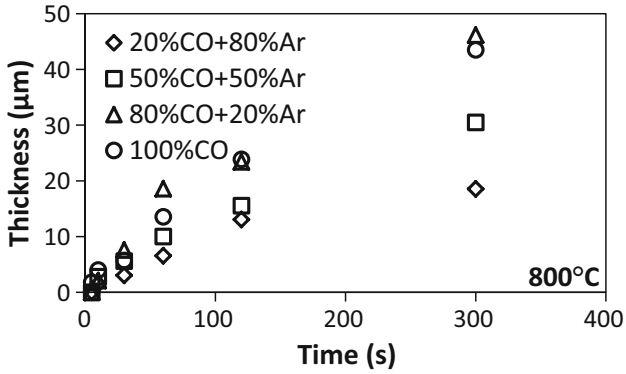

Fig. 17—Nickel metal product thickness as a function of time on reduction of NiO in CO/Ar gas mixtures at 1073 K (800 °C) (PCO + PAr = 1 atm.).

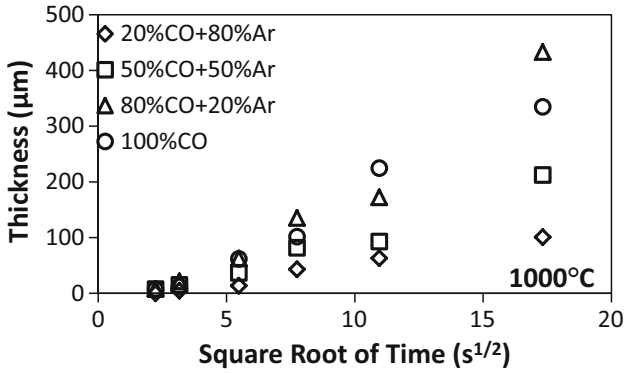

Fig. 18—Nickel metal product thickness as a function of $(time)^{0.5}$ on reduction of NiO in CO/Ar gas mixtures at 1273 K (1000 °C) (PCO + PAr = 1 atm.).

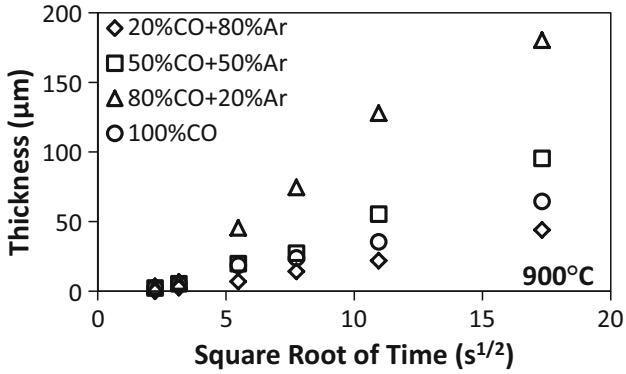

Fig. 19—Nickel metal product thickness as a function of $(time)^{0.5}$ on reduction of NiO in CO/Ar gas mixtures at 1173 K (900 °C) (PCO + PAr = 1 atm.).

lowered. In contrast, the thermodynamic driving is progressively reduced in CO/CO_2 gas mixtures with the decreasing CO partial pressure. The differences in behavior between the CO/CO_2 and CO/Ar systems increase as the temperature decreased.

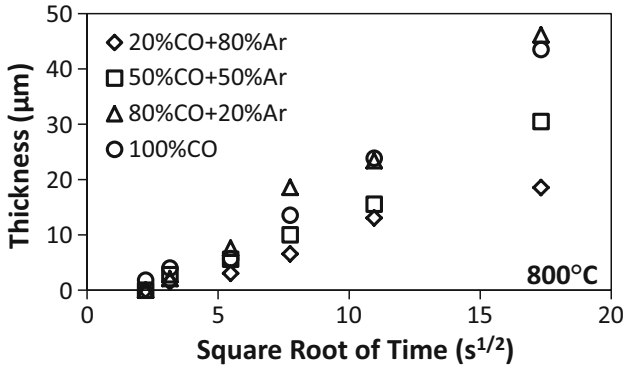

Fig. 20—Nickel metal product thickness as a function of $(time)^{0.5}$ on reduction of NiO in CO/Ar gas mixtures at 1073 K (800 °C) (PCO + PAr = 1 atm.).

In contrast to previous research undertaken using porous powder compacts with relatively small grain size, using dense NiO and this sectioning technique enabled the effect of product thickness on reaction rate to be clearly identified. It can be seen from Figures 15 through 17 that the reduction rates decrease as the time progresses and as the product thickness increases. The product thickness as a function of time to the power 0.5 are given in Figure 18 through 20; the linear relationships in these graphs indicating the reduction in each case may be described by parabolic rate equations of the form, $(thickness)^2 = kt$.

3. *$CO/CO_2/Ar$*

For all samples reduced in $(CO + CO_2)/(CO + CO_2 + Ar) = 1/4$ at 873 K to 1273 K (600 °C to 1000 °C) for ΔG − 150, − 120, − 90, − 60 kJ mol^{-1}, dense nickel layers were formed on the oxide surface. The growth rates of these layers were so low that they could not be accurately measured using the sectioning technique.

IV. DISCUSSION

It has been shown through the microstructural and kinetic studies undertaken in the present study that a number of different product structures can be formed and different behaviors can occur on reduction in CO/CO_2 gas mixtures depending on temperature and gas conditions. For convenience, in the following discussion, the reactions in particular ranges of conditions will be examined before bringing them together to describe the whole system.

A. *1073 K to 1273 K (800 °C to 1000 °C)*

In the temperature range from 1073 K to 1273 K (800 °C to 1000 °C) in CO/CO_2, two distinct final product structures were formed; dense nickel, which was formed as a layer on the original dense NiO, and a porous nickel product. The dense nickel layers were

formed under conditions of low thermodynamic driving force for reduction, which also corresponds to low CO partial pressure in the CO/CO_2 gas mixtures.

The microstructural information obtained from samples reduced for short reaction times at these temperatures indicates that, in all cases from (conditions A–E) an initial dense layer of nickel is formed; the porous product morphology is subsequently developed as the result of a separate mechanism. To demonstrate that this multistep, or discontinuous growth mechanism, is possible, an experiment was undertaken in which the gas conditions present at the sample outer surface were changed, while the sample was still at the same temperature. Figure 8 shows an example of the surface structure of the sample, following initial reduction at 1273 K (1000 °C) under condition E for 30 seconds, followed immediately, while still remaining at the same temperature, by reduction under gas condition A. It has previously been shown in this study that reduction at 1273 K (1000 °C), at condition E, will result in the formation of a dense nickel metal layer. It is clear from Figure 8 that most of the sample surface is covered with dense nickel metal layer. The original metal nuclei and NiO grain boundaries are clearly visible. The metal layer is, however, not completely flat; rather it appears to be covered by a network of circular raised caps, only some of which have associated with the pores. There are also pores in what appear to be the original NiO grain boundaries. While under the original condition having the dense nickel layer the reduction rate was slow, following the change to the new condition, with the high reduction potential, a porous nickel product structure (similar to that shown in Figure 7) was formed, and the complete reduction of the sample was rapidly attained.

The experiments indicate that in the temperature range from 1073 K to 1273 K (800 °C to 1000 °C) in CO/CO_2, the predominant reduction mechanism involves a discontinuous process involving first the formation of dense nickel metal layers on the NiO, and then the breakdown of this layer by bursting of the thin film. This mechanism is analogous to the proposed mechanism for the reduction of wustite ($Fe_{1-y}O$) with CO/CO_2[7] and NiO by H_2/H_2O.[8] In these previous studies, it was proposed that the breakdown was the result of a number of reaction steps involving chemical reaction at the gas/nickel metal sources to produce H or C, the diffusion of these species through the dense metal layer, and the subsequent reaction at the Ni/NiO interface. The formation of critically sized nuclei results in the formation of gas bubbles at the metal/metal oxide interface. The formation of the gas and the expansion of the bubbles lead to the formation of the circular caps in the nickel layer; some of these caps burst under pressure and provide pathways for the bulk gas to the underlying NiO. Thus, the reaction cycle is repeated.

The results of the present study indicate that, at all temperatures in the range from 1073 K to 1273 K (800 °C to 1000 °C), the growth rate of the product layer increases approximately linearly with the increased CO partial pressure if the critical CO pressure has been achieved at each temperature and decreases gradually over time. Figures 18 through 20 for reduction in CO/Ar gas mixtures show that the product thickness *vs* time relationships follow a parabolic rate law. Given the increased tortuosity and limited connected pathways through successive chambers within the porous product layer, it might reasonably be expected that there is increased resistance to transfer of gas through the porous product as the layer thickness increases. Normalization of these parabolic rate data with respect to CO pressure shows that the apparent rate constants are higher for the lower CO partial pressures. This observation might be explained by the sintering of the porous nickel product layer following its formation, increasing the effective pore size, and reducing the resistance to gas diffusion. Changes in pore size in the nickel metal product have previously been reported on reduction of NiO in H_2.[8]

From Figure 11, it can be seen that the initial rate of reaction in CO/CO_2 gas mixtures above approximately 873 K (600 °C) decreases before increasing again, such that the apparent reduction rate of reduction in CO at 873 K (600 °C) is approximately equal to that at 1123 K (850 °C). This observation may explain the results by Reference 2 who reported the apparent rate constant was independent of temperature between 953 K and 1069 K (680 °C and 796 °C), and similar results were reported by Reference 3.

B. *Reduction at 973 K (700 °C) and Below*

The microstructural and kinetic information obtained at temperatures of 973 K (700 °C) and below indicate that the reduction can take place through several different reaction mechanisms depending on the process conditions. At low thermodynamic driving forces at these temperatures, a dense nickel product layer is observed. The overall rates of reduction of NiO when the dense nickel metal layers are formed are extremely slow. At high reduction potentials, at temperatures between approximately 873 K and 973 K (600 °C and 700 °C), the microstructural evidence (see Figures 2 through 5) indicates that reduction takes place through a continuous pore growth mechanism. The appearance of the continuous growth morphology corresponds to increases in apparent reaction rate (see Figure 11) relative to those observed with the dense metal layer and discontinuous breakdown mechanisms. At temperatures below 873 K (600 °C) in CO/CO_2 gas mixtures, the rates are again extremely slow and a dense nickel product layer is formed at all gas conditions.

The microstructural and kinetic observations provide important clues as to the reaction mechanisms occurring in this and analogous gas/metal/metal oxide systems. These issues will be explored further in the following paragraphs.

Starting with the information available on the sequence of reactions taking place on reduction of NiO as a function of reaction time for temperatures at 973 K (700 °C) and below in CO-containing gas mixtures. Figure 2(a) shows that the initial smooth, polished NiO surface becomes facetted and pitted on exposure to the reaction gas. The isolated facetted pits (approximately 1 μm diameter) appear to be the result of selected

removal of oxygen from the surface; these are potentially associated with line defects in the crystal (screw dislocations) that emerge from the bulk crystal and provide preferential sites for reaction on the oxide surface.[9] The shape of the pits reflects the underlying cubic crystal structure of NiO and the relative surface energies associated with planes within the crystal.

Also formed are smaller pits that are distributed across the whole of the oxide surface. These pits are of the order of 100 to 200 nm in diameter. Based on previous studies of gas oxide reaction systems,[10,11] it is argued that these pits are in fact nascent pores or local instabilities forming at the gas/solid interface. The removal of oxygen atoms from the NiO surface by chemical reaction with the gas phase results in a local accumulation of excess nickel ions at the gas/solid interface. The resulting concentration gradient leads to diffusion of nickel ions into the bulk oxide and the development of local instabilities in the moving oxide surface. NiO, however, has a limited range of stoichiometry,[12] and the build-up of excess nickel in the bulk oxide as reduction proceeds leads to reduced driving force for instability growth, and eventually the instability growth stops.

The formation of metallic nickel nuclei on the oxide surface establishes important new reaction mechanisms and pathways in the system: (i) the metal can act as a sink for excess nickel ions generated by reaction of the gas with the NiO, and (ii) oxygen can diffuse onto the nickel metal surface and react with the adsorbed CO gas species. These steps are analogous to the reaction of adsorbed hydrogen on NiO during reduction[13]; however, this is not taking place on a planar surface rather in association with the curved surface at the pore tip. Both of these mechanisms enhance the overall rate of oxygen removal in the vicinity of the Ni/NiO interface and the pore tip, and hence the pore tip growth velocity.

The shape of the gas pores depends on the effective driving force for reduction. At relatively low driving forces, the pores are largely cellular in structure, with no or few relatively few side arms. As predicted from stability criteria, the single pore tips can divide into two to accommodate changes in diffusion field ahead of the pore tip.[14] With this pore geometry, the growth of the nickel over the oxide surface results in the formation of a layer of dense nickel metal on the surface of the pores. Provided the conditions for continued instability growth are met, the metal layer approaches but does not cover the pore tip; the pore tip radius will adjust to ensure the pore tip stays ahead of the metal. The smaller the pore tip radius, the greater the tip velocity. The removal of excess nickel ions from the pore tip takes pace primarily through volume diffusion through the oxide in the region of the gas/oxide interface. The steady-state growth of the pore tip represents a balance between the rates of the chemical reactions, *i.e.*, between gas and oxide, and the mass-transfer fluxes in the region of the pore tip, which take place through surface, and volume diffusion.

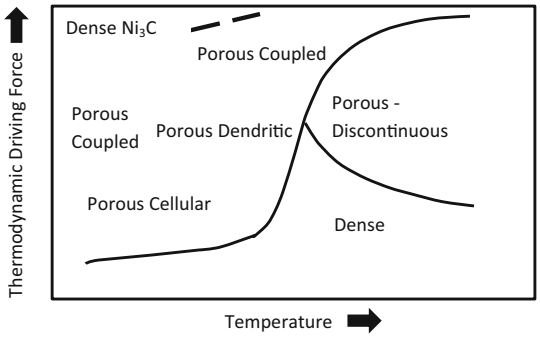

Fig. 21—Schematic morphology map indicating the proposed mechanisms of growth of nickel metal on reduction of NiO in CO/CO_2 gas mixtures ($PCO + PCO_2 = 1$ atm.).

At higher thermodynamic driving forces, dendritic pores (pores having a main stem with side arms forming in the pore walls) are created in the oxide ahead of the nickel metal layer. The pore diameter and spacing decreases with the increasing driving force at a given reaction temperature; leading to multiple pore stems that move progressively into the oxide. Under the conditions of high driving forces and low mobility of metal ions in the solid oxide (low volume diffusion coefficient), a planar overall interface structure is developed; the structure resembles a rod or lamellar structure of gas pores and nickel metal product. To maintain these growth structures, it is necessary to provide sufficiently high thermodynamic driving forces to drive not only the chemical reaction but also the transfer of excess nickel ions though surface diffusion across the gas/oxide interface.

In the case of reduction with CO/CO_2 gas mixtures, there is the potential formation of solid C and Ni_3C rather than Ni metal. The critical CO concentrations above which C and Ni_3C are formed in CO/CO_2 gas mixtures at 1 atm. total pressure are given in Table I. For example, the limiting conditions for C and Ni_3C formation are calculated to be approximately 9 pct CO and 99.5 pct CO, respectively, in CO/CO_2 gas mixtures at 1 atm. total pressure at 873 K (600 °C),[6] and these critical CO concentrations decrease with the decreasing temperature. In the present study, no carbon deposition was observed under any of the gas conditions and times studied, even though C was thermodynamically favored in some of these. This is somewhat surprising since nickel metal has been shown to catalyze the carbon deposition reaction.[15] The coincidence of the lower temperature and gas composition of formation of porous nickel with the limiting conditions for the formation of nickel carbide provides support for the view put forward by Reference 1 that the formation of the carbide inhibits the growth of the nickel product. This inhibition by Ni_3C could be due to the significantly reduced rates of chemical reaction between adsorbed CO and O on the modified nickel surface.

The chemical reactions and mass-transfer processes are all thermally activated processes, so it is to be expected that the conditions for instability formation will change with temperature for a given reaction system. Based on the observations in the present study and the proposed reaction mechanisms, the ranges of conditions, for which the different mechanisms might be expected to be predominant for CO/CO_2 gas mixtures at 1 atm. total pressure, are shown schematically in Figure 21.

C. *Comparison with NiO Reduction in H_2*

In the previous studies of reduction of NiO with H_2 and H_2/H_2O gas mixtures,[1,4] similar inflexions of growth rate with temperature to those noted in the present study were observed, *i.e.*, a rate minimum was observed at approximately 973 K (700 °C) and associated change in nickel product structure. Dense nickel metal layers were formed at ΔG at between − 30 and − 60 kJ mol^{-1} O_2.[8]

A two-stage reduction that involved an initial reduction of NiO at 1273 K (1000 °C) in 5 pct H_2-H_2O for 30 minutes to form an initial dense nickel product on the surface and a subsequent reduction using 100 pct (1 atm.) was carried out.[16] After the first stage, a dense nickel metal product layer was formed. After reduction in 100 pct hydrogen, the surface was found to be ruptured allowing gas access to the underlying NiO. This observation is exactly analogous to that seen in the present study with CO gas as shown in Figure 8.

Given the analogous behavior observed in different systems, the summary of reaction mechanisms shown in Figure 21 may also provide the template for describing on reduction of NiO with hydrogen[4,17–21] and similar metal/metal oxide reaction systems,[22] *e.g.*, CoO,[23] Cu_2O,[1] FeO.[24]

V. SUMMARY

The examination of partially reduced samples of dense NiO samples treated in CO/CO_2 and CO/Ar gas mixtures has revealed that the resulting nickel metal product can be obtained by three different mechanisms and form three different product structures. (i) A dense nickel product: The nucleation and spreading of nickel metal across the NiO surfaces result in the formation of dense nickel layers on the NiO—physically separating the reactant gas from the underlying NiO. (ii) A porous nickel product having continuous open cellular and dendritic pores: The formation of instabilities and gas pores in the oxide results in the continuous growth of porous Ni product; the porous nickel product enables continuous exchange of gas species between the bulk gas and the Ni/NiO interface and continuous contact between the gas phase and the NiO. (iii) A porous nickel product having discontinuous pore structures: This structure is created through a two-stage, iterative process involving the formation of a dense Ni layer and then physical rupture or breakdown of this layer.

Morphology maps have been created to identify the range of conditions under which these different product structures are formed for CO/CO_2 and CO/Ar gas mixtures and temperatures between 873 K and 1273 K (600 °C and 1000 °C).

The kinetics of reduction of NiO are shown to be directly related to the product structures and structures of the reaction interfaces; both product structures and rates of reaction are shown to be dependent on gas composition and reaction temperature.

The study has provided further insight into the reaction mechanisms taking place in gas/solid reaction systems. The need to consider separately, the different effects of reactant gas composition, partial pressure, and thermodynamic driving force for reduction in characterizing these reactions, has been demonstrated.

ACKNOWLEDGMENTS

The authors would like to acknowledge the financial support for this project from the Australian Research Council (ARC) Discovery program. The authors would also like to acknowledge the facilities, and the scientific and technical assistance provided by the Australian Microscopy & Microanalysis Research Facility at the Centre for Microscopy and Microanalysis, The University of Queensland.

REFERENCES

1. H. Mine, M. Tokuda, and M. Ohtani: *Nippon Kinzoku Gakkaishi*, 1970, vol. 34 (8), pp. 814–20.
2. J.H. Krasuk and J.M. Smith: *AIChE J.*, 1972, vol. 18 (3), pp. 505–12. https://doi.org/10.1002/aic.690180308.
3. J. Szekely and C.I. Lin: *Metall. Mater. Trans. B*, 1976, vol. 7, pp. 490–92.
4. T. Hidayat, A. Rhamdhani, E. Jak, and P.C. Hayes: *Metall. Mater. Trans. B*, 2009, vol. 40B, pp. 1–16.
5. S.P. Matthew, T.R. Cho, and P.C. Hayes: *Metall. Trans B*, 1990, vol. 21B, pp. 733–41.
6. FactSage: FACTweb, www.crct.polymtl.ca/.
7. D.H. St. John, S.P. Matthew, and P.C Hayes: *Metall. Trans B.*, 1984, vol. 15B, pp. 701–08.
8. T. Hidayat, A. Rhamdhani, E. Jak, and P.C. Hayes: *Metall. Mater. Trans. B*, 2009, vol. 40B, pp. 462–73.
9. P.C. Hayes: *Metall. Trans B.*, 1984, vol. 15B, pp. 519–24.
10. L. von Bogdandy and H-J. Engell: *The Reduction of Iron Ores—Scientific Basis and Technology*, Springer, Berlin, 1971.
11. P.C. Hayes: *Metall. Mater. Trans. B*, 2011, vol. 41 (1), pp. 19–34.
12. P. Kofstad: *Nonstoichiometry, Diffusion, and Electrical Conductivity in Binary Metal Oxides*, Wiley-Interscience, New York, 1972.
13. W. Pluschkell and B.V.S. Sarma: *Arch. Eisenhuttenwes.*, 1974, vol. 45 (1), pp. 23–31.
14. W. Kurz and D.J. Fischer: *Fundamentals of Solidification*, 4th ed., Trans Tech Publications, Aedermannsdorf, 1998.
15. D.J. Young: *High Temperature Oxidation and Corrosion of Metals*, 2nd ed., Elsevier, Oxford, 2016.
16. T. Hidayat, A. Rhamdhani, E. Jak, and P.C. Hayes: *Metall. Mater. Trans. B*, 2009, vol. 40B, pp. 474–89.
17. A.H. Rashed and Y.K. Rao: *Chem. Eng. Commun.*, 1996, vol. 156, pp. 1–30.
18. J.T. Richardson, R. Scates, and M.V. Twigg: *Appl. Catal. A Gen.*, 2003, vol. 246, pp. 137–50.
19. T.A. Utigard, M. Wu, G. Plascencia, and T. Marin: *Chem. Eng. Sci.*, 2005, vol. 60 (7), pp. 2061–68.

20. T. Hidayat, A. Rhamdhani, E. Jak, and P.C. Hayes: *Minerals Eng*., 2007, vol. 21 (2), pp. 157–66.
21. M.A. Rhamdhani, E. Jak, and P.C. Hayes: *Metall. Mater. Trans. B*, 2008, vol. 39B, pp. 218–33.
22. P.C. Hayes: *Mineral Process. Extract. Metall. Rev*., 1992, vol. 8, pp. 73–94.
23. K.R. Lilius: *Acta Polytech. Scand*., Ch. 117–124, 1974.
24. D.H. St John, S.P. Matthew, and P.C. Hayes: *Metall. Trans B*., 1984, vol. 15B, pp. 709–17.